



ELSEVIER

Tectonophysics 354 (2002) 49–70

TECTONOPHYSICS

www.elsevier.com/locate/tecto

Aftershock sequences in the mid-ocean ridge environment: an analysis using hydroacoustic data

D.R. Bohnenstiehl^{a,*}, M. Tolstoy^a, R.P. Dziak^b, C.G. Fox^c, D.K. Smith^d

^aLamont-Doherty Earth Observatory of Columbia University, 61 Route 9W, Box 1000, Palisades, NY 10964-8000, USA

^bCooperative Institute for Marine Resources Studies, Oregon State University/National Oceanic and Atmospheric Administration, Newport, OR 97365, USA

^cNational Oceanic and Atmospheric Administration/Pacific Marine Environmental Laboratory, Newport, OR 97365, USA

^dWoods Hole Oceanographic Institution, Woods Hole, MA 02543, USA

Received 19 September 2001; accepted 24 May 2002

Abstract

Hydroacoustic data from autonomous arrays and the U.S. Navy's Sound Surveillance System (SOSUS) provide an opportunity to examine the temporal and spatial properties of seismicity along portions of the slow-spreading Mid-Atlantic Ridge (MAR), intermediate-spreading Juan de Fuca Ridge (JdFR) and fast-spreading East Pacific Rise (EPR). Aftershock and foreshock events are selected from the hydroacoustic earthquake catalog using single-link cluster (SLC) analysis, with a combined space–time metric. In the regions examined, hydroacoustic data improve the completeness level of the earthquake catalog by ~ 1.5 – 2.0 orders of magnitude, allowing the decay constant, p , of the modified Omori law (MOL) to be determined for individual sequences. A non-parametric goodness-of-fit test indicates six of the seven sequences examined are described well by a MOL model. The p -values obtained for individual ridge and transform sequences using hydroacoustic data are larger than that previously estimated from the analysis of a stacked sequence generated from teleseismic data. For three sequences along the Siqueiros, Discovery and western Blanco Transforms, p -values are estimated to be ~ 0.94 – 1.29 . The spatial distribution of aftershocks suggests that the mainshock rupture is constrained by intra-transform spreading centers at these locations. An aftershock sequence following a $7.1M_s$ thrust event near the northern edge of the Easter Microplate exhibits $p = 1.02 \pm 0.11$. Within the sequence, aftershocks are located to the north of a large topographic ridge, which may represent the surface expression of the shallow-dipping fault that ruptured during the mainshock. Two aftershock sequences near $24^\circ 25' N$ and $16^\circ 35' N$ on the MAR exhibit higher p -values, 1.74 ± 0.23 and 2.37 ± 1.65 , although the latter estimate is not well constrained because of the small number of aftershocks. Larger p -values along the ridge crest might reflect a hotter thermal regime in this setting. Additional monitoring, however, will be needed to determine if p -value differences between the ridge and transform sequences are robust. A 1999 sequence on the Endeavour segment of the JdFR, which has been correlated with changes in the hydrothermal system, is described poorly by the MOL model. The failure of the MOL model, the anomalously large number of earthquakes within the sequence and absence of a clearly dominant mainshock are inconsistent with aftershock activity and the simple tectonic origin that has been proposed previously for this sequence.

© 2002 Elsevier Science B.V. All rights reserved.

Keywords: Earthquake sequence; Omori law; Endeavour segment; Easter Microplate; Oceanic transform; Normal fault

* Corresponding author. Tel.: +1-845-365-8382; fax: +1-845-365-8168.

E-mail address: del@ldeo.columbia.edu (D.R. Bohnenstiehl).

1. Introduction

The clustering of earthquakes has been long recognized in the mid-ocean ridge environment (e.g., Sykes, 1970; Francis and Porter, 1971). The limited detection capabilities of global seismic networks and the dearth of large magnitude earthquakes in this setting, however, have made it difficult to examine fully the temporal and spatial properties of ridge seismicity. Using the improved detection capabilities of hydroacoustic monitoring (Fox et al., 1994), we examine the properties of several earthquake sequences having a probable tectonic origin—those characterized by a large mainshock and a rapid decay rate of aftershocks through time. These sequences have been observed to occur along mid-ocean ridge spreading centers and oceanic-transform faults associated with the slow-spreading (~ 15 mm/year half-rate) Mid-Atlantic Ridge (MAR), intermediate-spreading (~ 30 mm/year half-rate) Juan de Fuca Ridge (JdFR) and fast-spreading (~ 55 mm/year half-rate) East Pacific Rise (EPR). In these settings, earthquakes may induce important changes within the hydrothermal system, influencing thermal budgets, chemical fluxes and biological communities (e.g., Sohn et al., 1999; Johnson et al., 2000, 2001). As such, an assessment of aftershock behavior is of broad interest to the Earth-science community.

Large magnitude earthquakes in both submarine and terrestrial settings commonly produce an aftershock sequence—a series of smaller events clustered around the mainshock in both space and time. Aftershocks are clearly a process of relaxing stress concentrations produced by the mainshock rupture (Scholz, 1990). The frequency of aftershock events per unit time $n(t)$ has been observed to follow a modified Omori law (MOL):

$$n(t) = K(c + t)^{-p}, \quad (1)$$

where K , c and p are all empirically derived constants. The rate constant p describes how rapidly the event rate decays in time, with a higher p -value indicating a faster decay. A median p -value of ~ 1.1 is reported for aftershock sequences in various parts of the world, with a range of ~ 0.6 – 2.5 (Utsu et al., 1995). K reflects the total number of events within the sequence and the size of the mainshock, and c reflects the rate

of activity within the earliest part of the sequence. When the decay rate of an aftershock sequence can be modeled with $c=0$ and $p=1$, Eq. (1) is known simply as the Omori law.

Of the above parameters, p has received the most attention, having been interpreted to reflect the properties of the fault system and surrounding lithosphere (e.g., Mogi, 1967; Kisslinger, 1996; Nanjo et al., 1998). No correlation with the magnitude of the mainshock is apparent (Utsu et al., 1995). Several authors have noted a possible correlation between heat flow (a proxy for hypocentral temperature) and p -value (Mogi, 1967; Kisslinger and Jones, 1991; Creamer and Kisslinger, 1993; Creamer, 1994; Kisslinger, 1996; Rabinowitz and Steinberg, 1998). Mogi (1967) suggested that the ability of rock to “flow” in higher temperature regions results in a rapid decrease in the residual stress following the mainshock, or higher p -value. Later modeling by Dieterich (1994), using rate- and state-dependent fault strength, indicated that $p>1$ may arise when the stress applied to the fault surface decreases with time following the mainshock.

Given the hotter thermal regime within the ridge setting, higher p -values might be expected in this environment. Quantifying the properties of mid-ocean ridge aftershock sequences, however, has proven difficult since most sequences contain few events of sufficient size to be detected by land-based seismic stations. Using superimposed sequences detected teleseismically (i.e., generating a set of aftershock occurrence times from multiple mainshocks), Davis and Frohlich (1991) estimated $p=0.928 \pm 0.024$ for the combined ridge-transform environment. This p -value is consistent with the heat flow hypothesis in that it is slightly higher than that obtained by stacking sequences from (lower temperature) shallow subduction zones 0.900 ± 0.009 (Davis and Frohlich, 1991). However, it is not clear that all of the sequences stacked actually conformed to the MOL or that ridge and transform sequences should have similar p -values. The inclusion of non-MOL sequences in a stacked sequence has been shown to yield lower p -values than would be obtained for individual MOL sequences within the same region (Nyffenegger, 1998). Below, we use hydroacoustic data, with a much lower detection threshold, to estimate the p -values of individual ridge and transform sequences.

2. Data and methods

2.1. T-wave data collection and processing

Data from autonomous underwater hydrophone (AUH) arrays along the northern MAR and central EPR and the U.S. Navy's *SOund SURveillance System* (SOSUS) distributed along the JdFR of the northeast Pacific Ocean are used to detect and locate submarine earthquakes (Fox et al., 1994, 2001) (Fig. 1). These systems record seismically generated Tertiary (T-) waves, which are acoustic waves that propagate over great distances within the ocean's *SOund Fixing And Ranging* (SOFAR) channel (Tol-

stoy and Ewing, 1950). The derived epicenters represent the region where T-wave energy is radiated into the water column. These locations reflect the epicenter of the earthquake, but potentially are biased by the bathymetry and character of the seafloor within the source region. However, monitoring along the MAR has shown that the locations of shallow hypocenter events do not appear to be systematically biased toward large-scale topographic features, such as the crest of the rift valley walls, and that T-wave locations are distributed across a range of seafloor depths even in areas with significant topographic relief (Smith et al., in press). T-wave locations have proven accurate enough to direct field parties to the

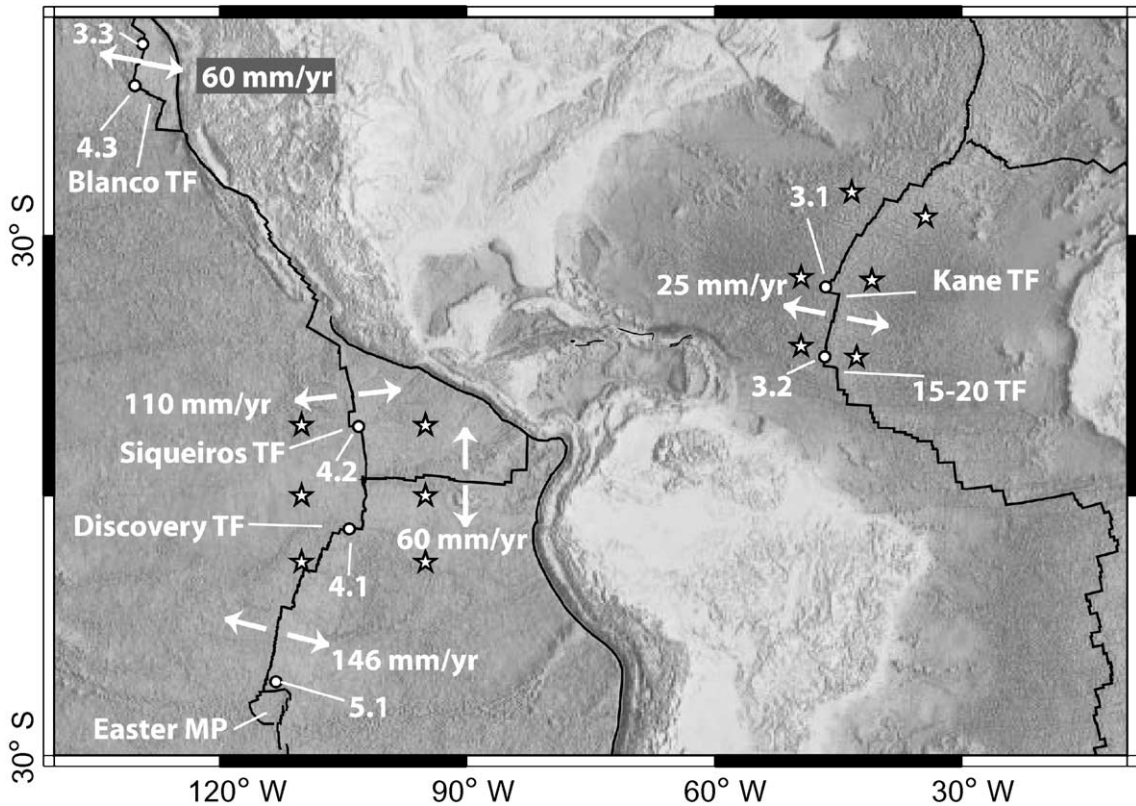


Fig. 1. Topographic map with the locations of the earthquake sequences examined marked with white circles (circles not to scale). Higher elevations are shown in light; lower elevations are shown in dark. Numbers refer to sections within the text where each sequence is described. Higher resolution images of the local bathymetry are shown in Fig. 3, with T-wave epicenters overlaid. Stars indicate the positions of moored autonomous hydrophones. Locations of SOSUS arrays within the northwest Pacific are classified. Plate boundaries marked with black lines. Full-spreading rates and spreading directions indicated by white arrows. Relevant transform faults (TF) and the Easter Microplate (MP) are labeled.

exact sites of submarine volcanism following several eruptions on northeast Pacific spreading centers (Fox, 1995; Dziak et al., 1996; Fox and Dziak, 1998; Dziak and Fox, 1999).

For each event, the peak energy of the T-wave signal is used as the arrival time. This portion of the signal has been suggested to radiate from the near epicenter region where the seafloor vibration is largest, as supported by the correlation between event depth and rise time (Schreiner et al., 1995; Slack et al., 1999). Following an analyst's identification of T-wave arrivals on three or more hydrophones, location analysis is accomplished using an iterative nonlinear least-squares method that minimizes the sum of the squared differences between the predicted and recorded arrival times at each instrument (Slack et al., 1999; Fox et al., 2001). Reported errors for the estimated parameters of latitude, longitude and origin time are based on point-source simulations calibrated using known sound sources. This approach suggests an accuracy of ~ 2 km at the 68% confidence level for events within the array; however, the T-wave source region is likely spread over an area of many km².

For T-wave events, acoustic magnitude, or source level (SL), is used as a measure of earthquake size. The SL is the acoustic power measured in decibels relative to micro-Pascals at 1 m, normalized by the sampling rate to yield spectral density (db re $\mu\text{Pa}/\sqrt{\text{Hz}}$ at 1 m) (Dziak et al., 1997; Dziak, 2001; Fox et al., 2001). Spectral amplitudes between 5 and 30 Hz are used since this band provides the optimum signal-to-noise ratio (Dziak et al., 1997). After each event is located, an independent estimate of the SL is calculated for each receiving hydrophone by adding a transmission loss factor that accounts for both spherical spreading from the seafloor into the sound channel and cylindrical spreading along the sound channel path. The mean SL and standard deviation of these estimates are cataloged.

For earthquakes located within one of the hydro-acoustic arrays and of sufficient size to be detected by land-based seismic stations, the large amplitude of the arriving T-waves may saturate the some or all of the hydrophone sensors. This clipping typically results in an underestimate of the SL and larger standard errors for these events. As a general rule for events within one of the hydroacoustic arrays, SL values >220 – 225 db should be considered suspect, and teleseismic

magnitudes should be used when available to assess the relative size of these earthquakes. We make use of the National Earthquakes Information Center's (NEIC) Preliminary Determination of Epicenters (PDE) catalog and the Prototype International Data Center's (PDIC) Revised Event Bulletin (REB). The latter presently is not available after 20 February 2000. As the dynamic range of the AUHs is improved during future deployments, the SL complications associated with clipping will be eliminated.

Information regarding source mechanism and hypocentral depth is not recovered presently from the T-wave data; however, in the near-ridge environment earthquake depths can be assumed to be <5 – 10 km (Bergman and Solomon, 1984). Moment tensor solutions are available for events having moment magnitude (M_w) >5.0 – 5.5 (Dziewonski et al., 1981), providing insight into the tectonics of the sequences examined. Details regarding the processing of SOSUS data can be found in Fox et al. (1994) and Dziak et al. (1997). Fox et al. (2001) provide a full description of AUH data reduction and describe the equatorial Pacific array. Smith et al. (in press) describe the Atlantic AUH array.

2.2. Magnitude of completeness and size–frequency distribution

In determining the parameters of the MOL (Eq. (1)), analysis is restricted to events larger than the magnitude of completeness (M_c)—the magnitude or source level above which the data set is complete. M_c is estimated from the size–frequency distribution, which over some range of event sizes can be described as:

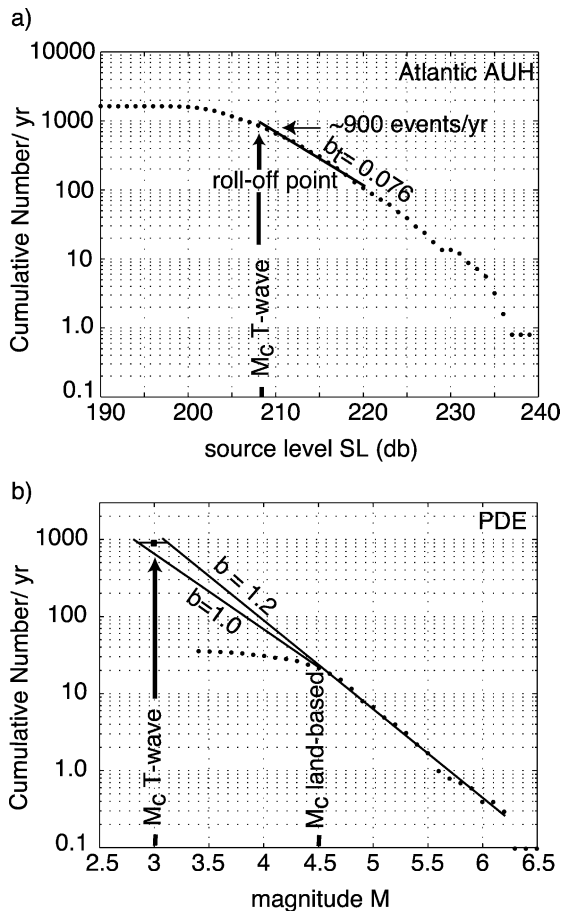
$$\log N(\text{SL}) = A - b_t \text{SL}, \quad (2)$$

where N is the number of events having size $\geq \text{SL}$, A is a constant dependent on the total number of events and b_t is analogous to b in the more familiar Gutenberg–Richter relationship.

The cumulative SL–frequency distribution of events within the Atlantic hydrophone array, between the Fifteen–Twenty and Oceanographer Fracture Zones and within 100 km of the ridge axis, is shown in Fig. 2a. M_c is identified subjectively as the source level at which the data depart from the relationship given in Eq. (2). The parameter b_t is estimated by a

least-squares fit of the cumulative source level data, for $M_c \leq SL \leq 220$ db. Data with $SL > 220$ db are excluded from the regression to account for clipping of the hydrophone sensors during the largest events. Inspection of MAR size–frequency data, indicates a departure from the predicted distribution at source levels $< \sim 208$ db. The 208-db level of the size–frequency roll-off (M_c) can be correlated with a seismic magnitude by extrapolating the long-term teleseismically observed distribution (Fig. 2b). This first-order approach indicates that the AUH data set is complete for events larger than $\sim 3.0 \pm 0.2 M$, with a number of smaller events also detected. A preferred magnitude scale (M) is used to account for the partial saturation of the m_b scale at magnitudes > 5 – 5.5 (Geller, 1976), with decreasing preference given to M_w , M_s and m_b . A similar analysis of the Pacific

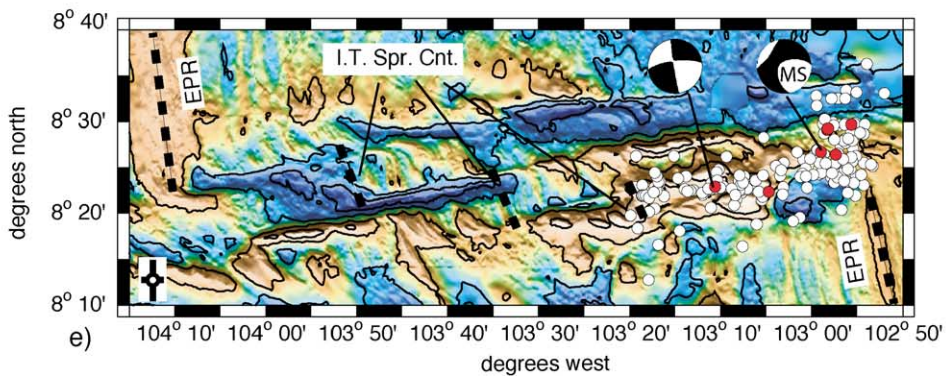
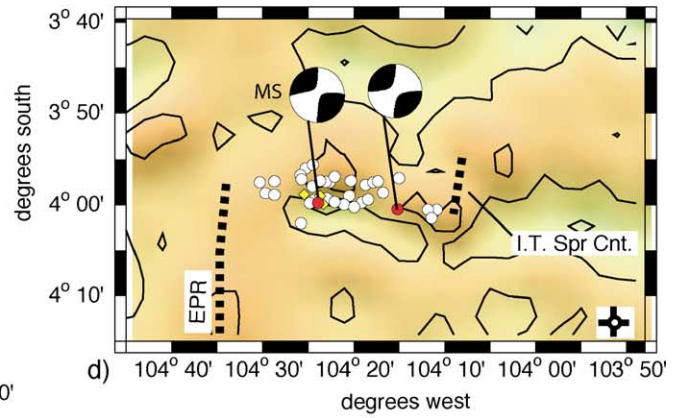
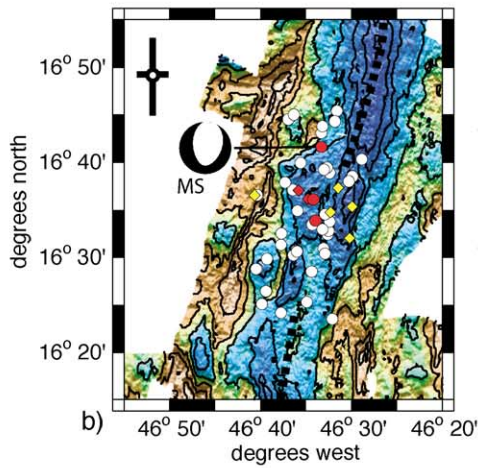
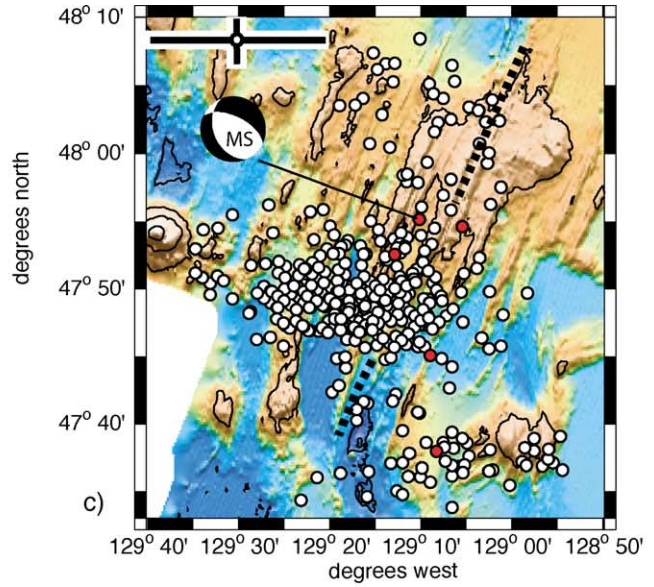
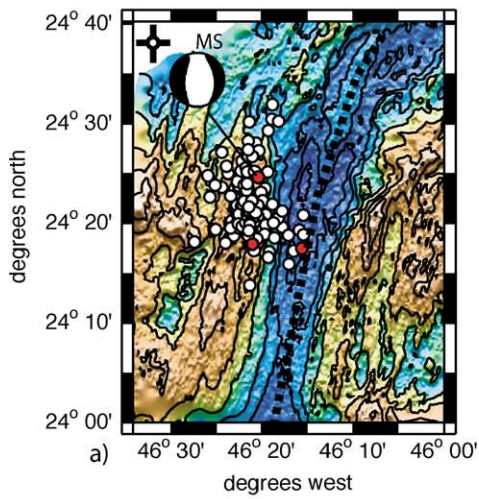
hydrophone array indicate the data are complete for events $\geq \sim 207$ db, which corresponds to a magnitude of $\sim 2.5 \pm 0.4 M$ in this setting. This M_c estimate is somewhat higher than the $\sim 1.8 M$ estimated in Fox et al. (2001) by extrapolating an empirical relationship derived for events in the range 4.0 – $4.7 M$. For the JdFR, cumulative-SL data roll off below ~ 204 db along the Endeavour Segment and ~ 207 db along the Blanco Transform, indicating a completeness level of $\sim 2.5 \pm 0.3 M$ for the SOSUS data. This is consistent with the estimate made by Fox et al. (1994) using a similar approach. Temporal and spatial variations in M_c may reflect mechanism-dependent differences in the efficiency of T-wave generation (Dziak, 2001; Park et al., 2001), variable ambient noise levels, instrument failure or local topographic blockage. To minimize these complications, M_c is determined for each individual sequence and aftershocks with $SL < M_c$ are removed prior to determining the decay parameters of the MOL.

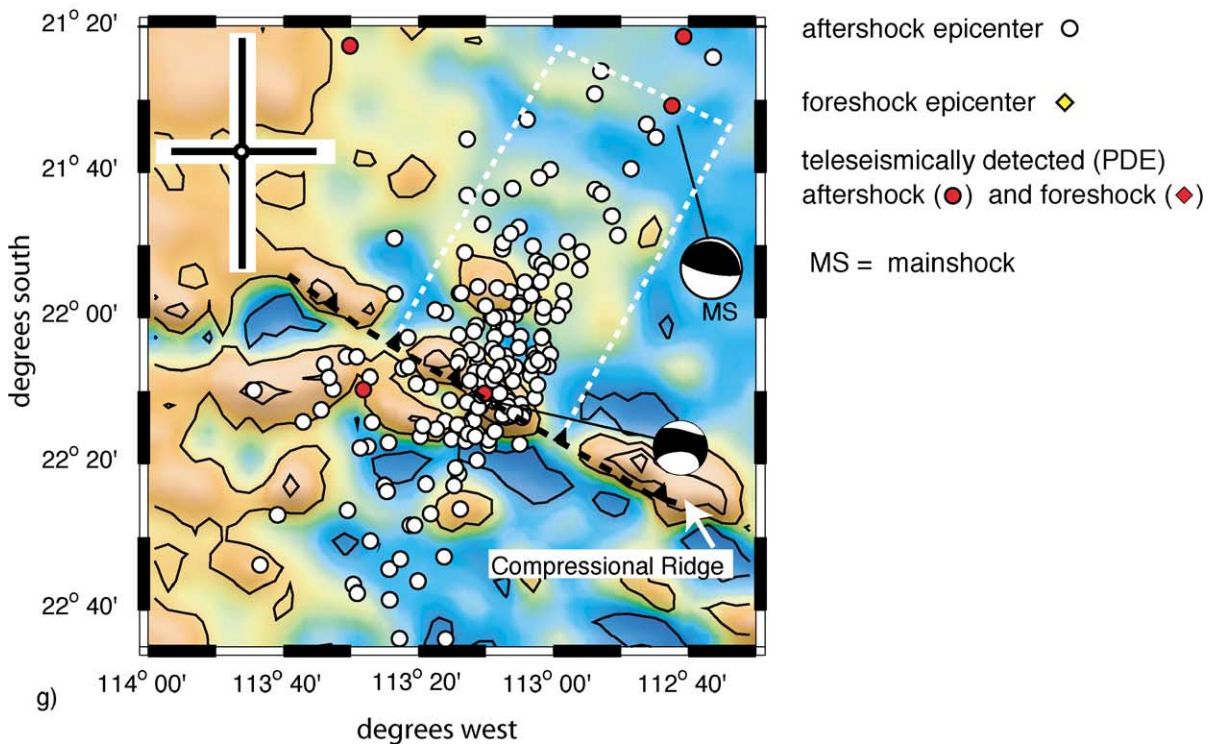
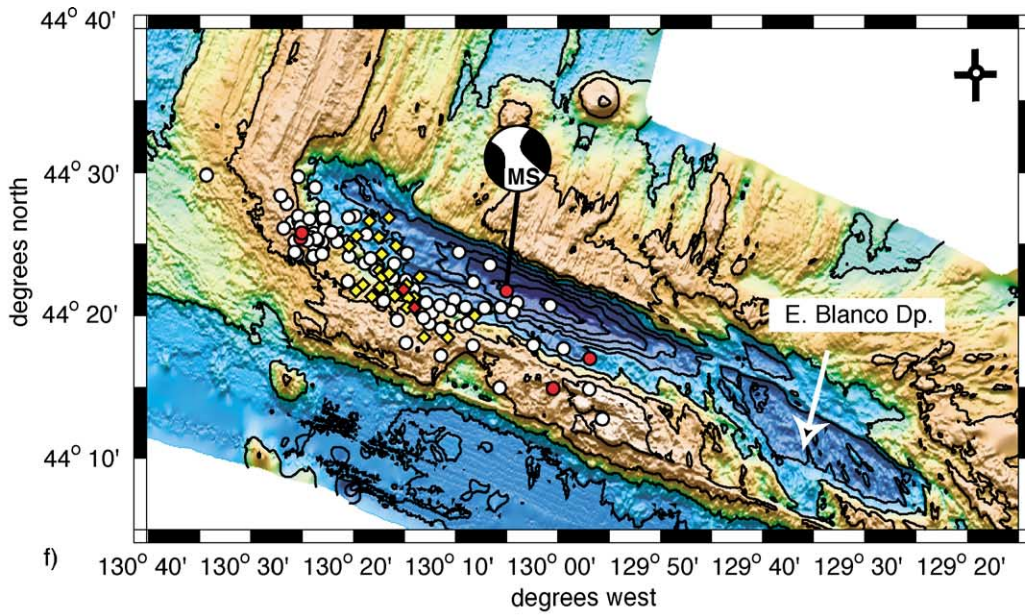


2.3. Identifying aftershocks

Large magnitude events were identified within each of the central Pacific AUH, northern Atlantic

Fig. 2. (a) Frequency–source level distribution of earthquake detected within 100 km of the ridge axis between the Fifteen–Twenty and Oceanographer Fracture Zones. Data recorded using the Atlantic AUH array. Source level in decibels is on the x-axis and cumulative number of events on the y-axis. Time interval March 1999–April 2000, with data normalized to 1 year. The cumulative frequency distribution adheres to the relationship given in Eq. (2) for events larger than ~ 208 db, or the largest ~ 900 events each year. The slope of the data (b_1) is estimated to be 0.076 by a least-squares regression of the data between 208 and 220 db. Data with $SL > 220$ db are excluded due to clipping of the hydrophone sensors. (b) Frequency–magnitude distribution of earthquake detected by land-based seismic station and located within 100 km of the ridge axis between the Fifteen–Twenty and Oceanographer fracture zones. Data recorded during a 10-year period (PDE catalog) and normalized to 1 year. To account for the saturation of the body-wave magnitude scale (m_b), preferred magnitudes (M) are given—with decreasing preference given to M_w , M_s and m_b values. The teleseismic data has a completeness level (M_c) of $\sim 4.5 M$. A b -value of 1.2 is obtained by least-square regression of the data with magnitude $> 4.5 M$. Extrapolating the distribution suggests that the 208 db level corresponds to a $\sim 3.2 M$ earthquake. Assuming $b = 1.0$ at lower magnitudes, suggests that the 208 db level is equivalent to $\sim 2.8 M$.





AUH and northeast Pacific SOSUS databases. Earthquakes occurring within 200 km and within 300 days after these potential mainshocks were extracted from the database. Aftershocks were then selected from this subset of events using a single-link cluster (SLC) algorithm (e.g., Frohlich and Davis, 1990). A space–time metric D is used to define the proximity of events relative to one another. This metric is defined as:

$$D = \sqrt{d^2 + B^2 \Delta_t^2}, \quad (3)$$

where d is the distance between two T-wave epicenters, Δ_t is the temporal separation between two events and B is a constant relating time to distance. The units of D are space–time km (ST-km). We adopt $B = 1$ km/day, after Davis and Frohlich (1991). Two events occurring simultaneously with a separation distance of 10 km, therefore, have the same D as two events that have coincident epicenters but occur 10 days apart. Once the proximity of events is determined they can be grouped together into binary clusters (clusters of two events). These clusters are then linked together into larger and larger clusters, forming a hierarchical tree. Aftershocks are then defined as events within a D_c -size (critical size) cluster containing the mainshock. SLC analysis is a natural choice for aftershock selection because it avoids subjective decision-making with regard to the spatial distribution and duration of the sequence,

allows for variable rates of background activity through the selection of D_c and requires no assumption as to the efficiency of event triggering, as is necessary when applying other clustering algorithms (e.g., Reasenber, 1985).

D_c is chosen based on the median link length within the catalog, D_1 . Davis and Frohlich (1991) have suggested $D_c = \beta_1 \sqrt{D_1} - \beta_2$, where $\beta_1 = 9.4$ ST-km^{1/2} and $\beta_2 = 25.2$ ST-km, as the value that correctly identified the greatest number of sequences in their analysis of synthetic earthquake catalogs. However, for small median link length this equation yields negative D_c values. Constraining $D_c = 0$ for $D_1 = 0$ in a similar analysis, Nyffenegger (1998) and Nyffenegger and Frohlich (2000) have suggested a choice of $D_c = 0.8D_1$. We apply this criterion, as well as a less conservative $D_c = 1.25D_1$, to all sequences. The latter accounts for potential bias due to the relatively short duration of the T-wave earthquake catalogs.

D_1 reflects the natural time–space density of epicenters within each region, as well the location and detection capabilities of the network. For the MAR AUH catalog, $D_1 = 13.0$ ST-km within the array. Within the SOSUS catalog, $D_1 = 9.5$ ST-km and $D_1 = 6.0$ ST-km for the Blanco and Endeavour regions, respectively. Within the EPR AUH catalog, $D_1 = 9.0$ ST-km. For the EPR dataset, only transform sections of the plate boundary are considered in determining D_1 , since much of the spreading axis is aseismic above the detection threshold of the AUHs.

Fig. 3. Bathymetric image and hydroacoustic locations for foreshocks and aftershocks selected using SLC analysis. Events selected using the $D_c = 0.8D_1$ criterion shown for all sequences, except f ($D_c = 1.25D_1$). Solid black crosses indicate the mean location errors (95% confidence intervals), as derived from point-source modeling. Dashed black lines indicate spreading centers. Harvard centroid-moment tensor solutions are shown, unless otherwise noted. (a) April 1999 MAR (Fig. 4). Events are located on the western bounding wall of the rift valley. They are clustered around the $5.9M_w$ normal-faulting mainshock with a spatial pattern that is elongate parallel to the structural fabric. (b) February 2000 MAR (Fig. 5). The mainshock is a $5.6M_w$ normal-faulting event. Aftershocks are located on the median valley floor and lower-most bounding walls. The trend of their spatial pattern is also parallel to the structural fabric. (c) June 1999 Endeavour Segment JdFR (Fig. 6). The sequence was initiated by a ~ 4.0 M event, which has normal-faulting focal mechanism (OSU moment tensor) (Johnson et al., 2000). The along-axis distribution, which is well constrained, is >2 times larger than it is for the normal-faulting sequences on the MAR. (d) August 1996 Discovery Transform EPR (Fig. 7). A $5.9M_w$ left-lateral strike–slip earthquake initiated the sequence. Aftershocks occur between the EPR axis and an intra-transform spreading center (I.T. Spr.Cnt.). (e) May 1998 Siqueiros Transform EPR (Fig. 8). Sequence contains two $5.8M_w$ left-lateral strike–slip events separated by 0.79 days. The first occurred near the eastern ridge-transform intersection and the second near $103^\circ 10' W$. Aftershock locations are bounded by the ridge axis and eastern most intra-transform spreading center. (f) June 2000 West Blanco Transform JdFR (Fig. 9). The mainshock event is a $6.3M_w$ right-lateral strike–slip earthquake that is preceded by numerous foreshocks. Aftershocks occur between JdFR and extensional East Blanco Depression. (g) September 1996 Easter Microplate (Fig. 10). The mainshock is a shallow north-dipping (15°) thrust earthquake (Delouis et al., 1998). Aftershocks are located to the north of a large compressional ridge, which may represent the surface expression of the fault that ruptured. Dashed white line is a projection of the possible rupture area inferred from the distribution of aftershocks. Note that this sequence occurs well outside the Pacific AUH array and therefore an elliptical error distribution is predicted with the long axis oriented away from the array (approximately NE–SW).

After events have been identified using SLC analysis, the SL–frequency distribution of the sequence is examined, and its M_c level is determined. In estimating the temporal decay parameters of the sequence (Section 2.4), analysis is restricted to events with $SL \geq M_c$. Our analysis is limited to those sequences having >20 aftershocks.

2.4. Estimation of decay parameters

The parameters of the MOL are estimated using the method of maximum likelihood. Consider a series of aftershock occurrence times $\{t_1, t_2, \dots, t_N\}$ within a time interval $[S, T]$, where $t=0$ corresponds to the time of the mainshock. Assuming that the aftershocks are distributed according to a non-stationary Poisson process with intensity function $\lambda(t) = n(t) = K(t+c)^{-p}$, an estimate of the parameters K, c and p is obtained by finding those values that maximize the logarithm of the likelihood function (Ogata, 1983):

$$L = \left\{ \prod_i^N \lambda(t_i) \right\} \exp \left\{ - \int_s^T \lambda(t) dt \right\}. \quad (4)$$

This maximization is carried out within the software package SAseis using a Fletcher–Powell optimization procedure (Utsu and Ogata, 1997). An estimate of the standard error associated with the maximum-likelihood estimate of each parameter is produced as a byproduct. See Ogata (1983, 1999) for an extended description of these techniques.

Identifying aftershocks within the initial time period following the mainshock may be difficult due to the mainshock coda and the complicated nature of aftershocks in the initial stages of the sequences. This will result in a biased estimate of

the MOL parameters if $S=0$ is assumed (Ogata, 1999). The cumulative-event data for each sequence are examined for the early portions of each sequence to determine S . If an abrupt change in event rate or

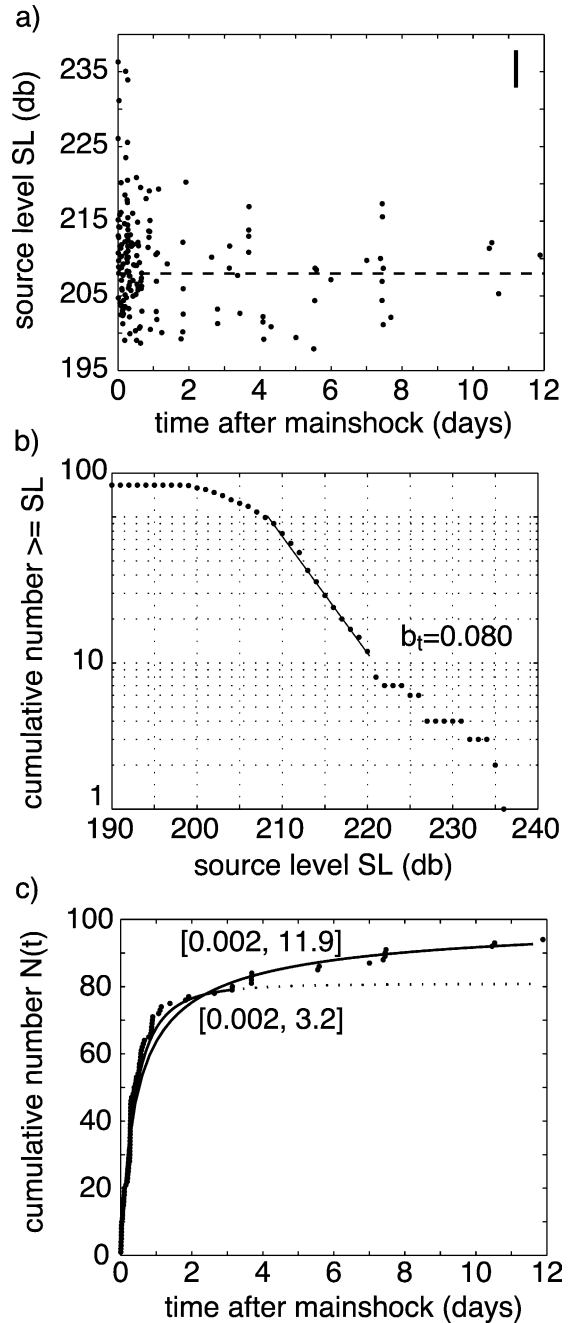


Fig. 4. Aftershock sequence initiated on 6 April 1999, near 24°25' N on the MAR. The events selected using the $D_c=10.5$ ST-km criterion are shown. (a) Source level vs. time relative to the mainshock. Vertical bar is the median source level error. Events with source levels ≥ 208 db (horizontal line) are used in determining the parameters of the MOL. (b) Cumulative-source level plot of aftershocks. $M_c=208$ db. $b_1=0.080$ (c) Cumulative number of events vs. time after the mainshock. Solid line is the predicted cumulative distribution for the maximum-likelihood estimates of the MOL parameters, as given in Table 1 (Dashed where extrapolated). The data are fit well by a MOL model.

other anomalous behavior is not identified near the beginning of the sequence, S is selected to provide the best relative fit to the data over the interval $[S, T]$ from a range of S values $\{0.001, 0.002, \dots 0.1\}$ and full duration T .

2.5. Goodness-of-fit

Typically, the relative fit of two competing aftershock models has been evaluated using the Akaike Information Criteria (AIC) (Akaike, 1973; Ogata, 1983):

$$\text{AIC} = -2\{\max \ln(L)\} + 2k, \quad (5)$$

where k is the number of free parameters (3 for a MOL model) and L is the likelihood function. However, only relative AIC values are meaningful, with smaller values indicating a better fit. Alternatively, the nonparametric Anderson–Darling statistic (Anderson and Darling, 1954; Lewis, 1961), which evaluates the deviation of the data from the best fitting model, has been used previously to test a number of proposed distributions (e.g., Frohlich, 1987; Willemann and Frohlich, 1987; Davis and Frohlich, 1991), including a MOL (Nyffenegger and Frohlich, 1998, 2000). In

keeping with these studies, we utilize this goodness-of-fit test to evaluate how closely the occurrence times of individual aftershocks resemble those in an ideally distributed sequence having the same population and duration.

For a sequence of N events occurring within the time interval $[S, T]$, the occurrence time of the i th event ($i=1, 2, \dots N$) is defined as t_i . The Anderson–Darling statistic can be written as:

$$A^2 = -N + \frac{1}{N} \sum_{i=1}^N (2i-1) [\ln(u_i) + \ln(1-u_{N+1-i})], \quad (6)$$

where u_i is the expected value of the cumulative density function (cdf) after time t_i . For a sequence of aftershocks obeying a MOL (Eq. (1)), the expected cdf is given by:

$$u_i = \frac{(t_i + c)^{1-p} - (S + c)^{1-p}}{(T + c)^{1-p} - (S + c)^{1-p}}. \quad (7)$$

Smaller values of A^2 indicate a better fit to the distribution. For $N > 8$, $A^2 = 0.50, 1.0$, and 2.49 repre-

Table 1
Properties of aftershock sequences associated with spreading centers

Sequence	D_c^a (ST-km)	$[S, T]^b$ (days)	N_u^c	p	c (days)	K	A^2 ^d
24°25' N MAR 06 Apr 99 5.9 M_w^e	10.5	[0.002, 11.9]	93	1.57 (0.25) ^f	0.23 (0.12)	25.6	1.19
		[0.002, 3.2]	79	3.57 (2.05)	0.98 (0.91)	196.3	0.99
		[0.002, 27.2]	94	1.74 (0.23)	0.29 (0.14)	29.1	0.98
16°35' N MAR 18 Feb 00 5.6 M_w^e	10.5	[0.01, 3.95]	21	2.37 (1.65)	0.49 (0.72)	11.6	0.60
		[3.95, 6.8]	7	1.26 (0.80)	0.05 (0.14)	1.3	0.50
		[0.01, 6.8]	28	2.17	0.37	8.2	0.64
					0.13	0.7	1.10
47°50' N Endeavour JdFR 8 Jun 99 3.4–4.5 M^e	4.8	[1.0, 13.2]	227	3.98 (1.25)	2.40 (1.71)	14,000	5.59
		[1.0, 13.7]	240	3.14 (0.80)	1.49 (1.12)	1800	5.94
	40 km ^g	[0.7, 13.7]	285	3.85 (1.08)	2.93 (1.65)	21,750	5.77
		[0.7, 76.8]	314	1.97 (0.16)	0.50 (0.30)	370	7.82
		[0.1, 76.8]	384	2.39 (0.22)	2.20 (0.53)	1760	14.29

^a Space–time metric used to select aftershocks using SLC analysis.

^b Time interval during which the data are modeled. Times are relative to mainshock time. The full duration data, as determined from SLC analysis, were modeled for all sequences. Numerous other time intervals, chosen by inspection of the aftershock data, were also modeled; only values relevant to the discussion are reported.

^c Number of aftershocks within the interval $[S, T]$ used in determining p , c and K .

^d Anderson–Darling statistic. Smaller values of A^2 indicate better fits to the MOL. Sequences with $A^2 < \sim 1.0$ are fit well by the MOL model.

^e Mainshock magnitude.

^f Standard error of the maximum likelihood estimation.

^g All events within 40 km and 80 days of the mainshock selected as aftershocks.

sents the 25%, 50% and 95% confidence levels, respectively (Lewis, 1961). Sequences with $A^2 < 2.0$ previously have been assumed to be consistent with a MOL, and those with $A^2 < 1.0$ have been considered to be fit well (Nyffenegger, 1998; Nyffenegger and Frohlich, 2000).

3. Spreading-center sequences

3.1. 24°25' N on the Mid-Atlantic Ridge—06 April 1999

An aftershock sequence was initiated by a $5.9M_w$ normal-faulting event at 04:51Z on 06 April 1999 near 24°25' N on the MAR. In addition to the mainshock, two aftershocks were reported by both the NEIC (PDE catalog) and PIDC (REB catalog) at 0.22 and 0.27 days following the mainshock, with an earlier aftershock at 0.03 days reported only by the PIDC. These seismically detected aftershock events have magnitudes in the $3.9\text{--}4.5m_b$ range. Events within the sequence cluster within the western wall of the rift valley. Aftershocks occur within 15–20 km of the epicenter of the mainshock, with a spatial pattern that trends parallel to the trend of the rift valley and the strike of the bounding-wall faults (Fig. 3a).

Using the $D_c = 10.5$ ST-km criterion, SLC analysis identified a total of 165 events during a ~ 12 -day period following the mainshock (Fig. 4) and 169 events during a period of ~ 33 days using the 16.0 ST-km criterion. No foreshocks were identified with either criterion. M_c is estimated to be 208 db, with

$b_t = 0.080$ (Fig. 4b). The sequence contains 95 events with $SL > M_c$ for $D_c = 10.5$ ST-km. Values of 1.57 ± 0.25 , 1.59 ± 0.30 and 3.57 ± 2.05 are obtained for p by fitting the data for a time interval of 11.9, 7.5 and 3.2 days, respectively (Table 1) (Fig. 4c). A^2

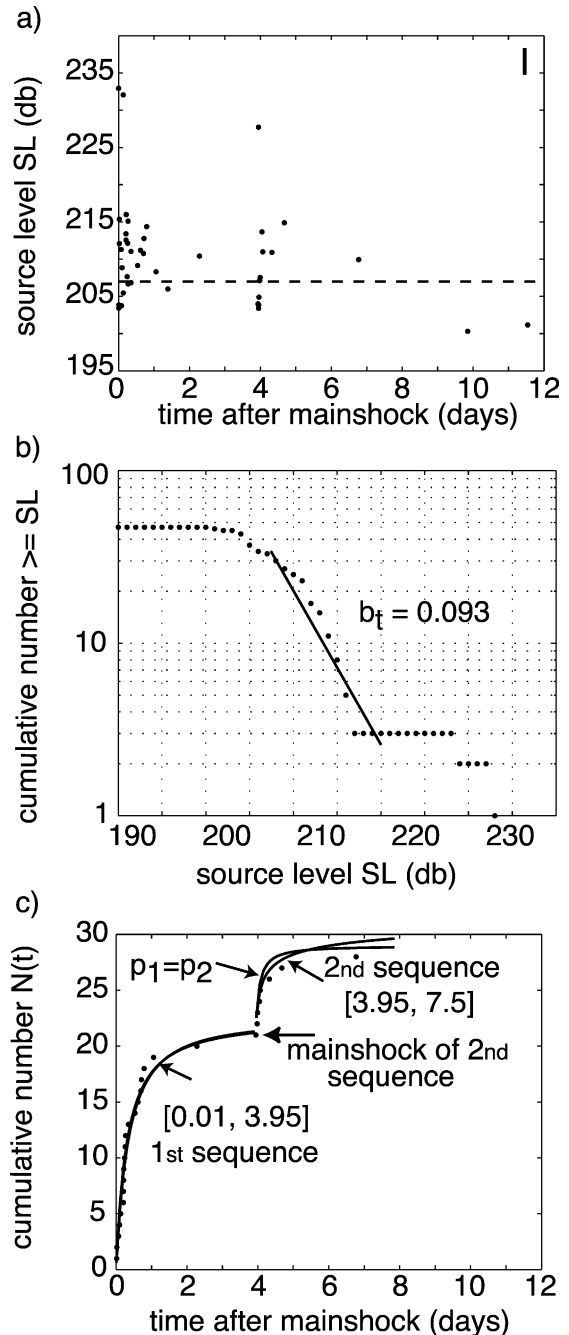


Fig. 5. Aftershock sequence initiated on 18 February 2000, near 16°35' N on the MAR. The events selected using the $D_c = 10.5$ ST-km criterion are shown. (a) Source level vs. time relative to the mainshock. Vertical bar is the median source level error. Events with source levels ≥ 207 db (horizontal line) are used in determining the parameters of the MOL. (b) Cumulative-source level plot of aftershocks. $M_c = 207$ db. $b_t = 0.093$. (c) Cumulative number of events vs. time after the mainshock. Solid line is the predicted cumulative distribution for the maximum-likelihood estimates of the MOL parameters, as given in Table 1 (Dashed where extrapolated). The data are fit well by a MOL model. A change in the occurrence rate of aftershocks is associated with a largest magnitude aftershock. The data are modeled as two independent sequences and as a composite event.

values are near 1.0, indicating that the data are consistent with a MOL model. Fitting the $D_c=16$ ST-km data gives a p -value of 1.74 ± 0.23 and a slight better fit than the full duration $D_c=10.5$ ST-km data (Table 1).

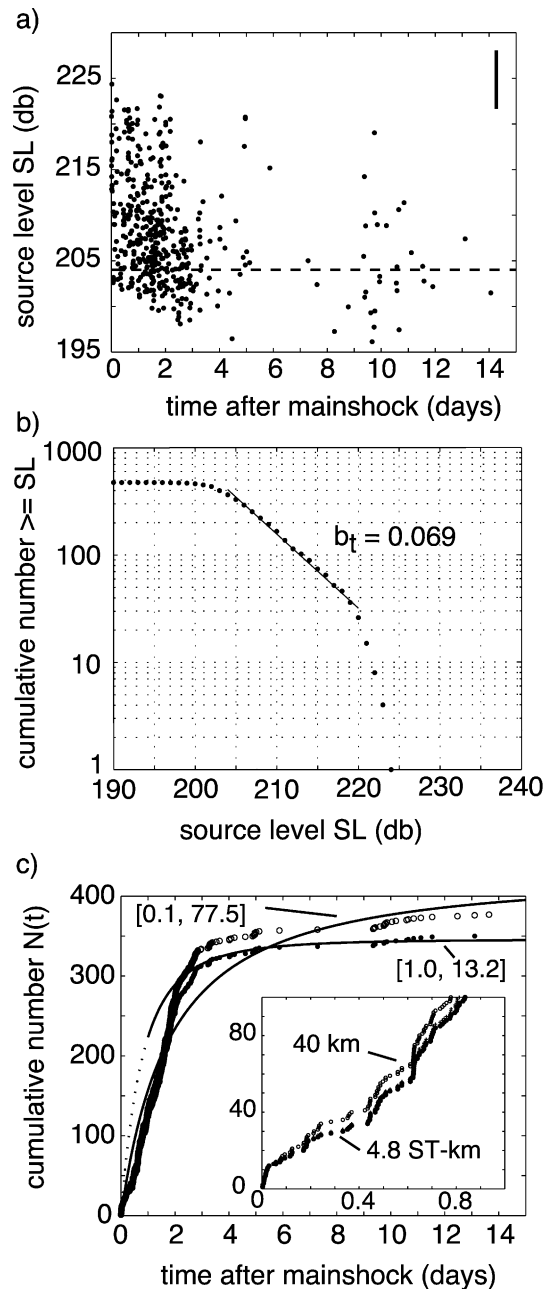
3.2. $16^\circ 35' N$ on the Mid-Atlantic Ridge—18 February 2000

A $5.6M_w$ normal-faulting earthquake occurred at 08:06Z on 18 February 2000. This mainshock event occurred within the third segment north of the Fifteen–Twenty Fracture Zone. It was located near the western edge of the valley floor at $16^\circ 35' N$, producing an aftershock sequence with events distributed across the valley floor and lower bounding walls (Fig. 3b). As observed for the April 1999 sequence, the spatial trend of aftershocks follows the structural trend of the axis. In addition to the mainshock, two aftershocks having magnitudes of 4.5 and $4.8m_b$ were detected by the NEIC at 0.13 and 3.95 days after the mainshock.

Using a $D_c=10.5$ ST-km criterion, SLC analysis identified 43 aftershocks with a duration of ~ 12 days (Fig. 5). For $D_c=16.0$ ST-km, 46 aftershocks having a duration of ~ 12 days were identified. M_c for the sequence is estimated to be 207 db, with $b_t=0.093$. Inspection of the cumulative event data (Fig. 5c) shows the cluster identified consists of two smaller sequences, with the second sequence initiated by a $4.8m_b$ event at 3.95 days. We model each sequence individually and then both sequences together as a composite sequence in which after-

shocks from the first mainshock contribute to the event rate of the second sequence. For the $D_c=10.5$ data, the p -value for the first sequence is determined to be 2.37 ± 1.65 for $t < 3.95$ days. Treating the second event independent of the first, p is estimated to be 1.26 ± 0.80 . Considering both sequences

Fig. 6. Earthquake sequence initiated on 8 June 1999, near $47^\circ 50' N$ on the Endeavour Segment of the JdFR. The events selected using the $D_c=4.8$ ST-km criterion are shown. (a) Source level vs. time relative to the mainshock. Vertical bar is the median source level error. Events with source levels ≥ 204 db (horizontal line) are used in determining the parameters of the MOL. (b) Cumulative-source level plot of aftershocks. $M_c=204$ db. $b_t=0.069$. (c) Cumulative number of events vs. time after the mainshock. Solid line is the predicted cumulative distribution for the maximum-likelihood estimates of the MOL parameters, as given in Table 1 (Dashed where extrapolated). Open circles show events within 40 km of the mainshocks. Solid dots show events selected using SLC analysis. A MOL model fits the data poorly, with anomalous behavior during the first day (see inset).



together, with a $p_1=p_2$ constraint, yields $p=2.17$. Analysis of the $D_c=16.0$ data yields nearly identical results. A^2 values indicate that these data are described well by the MOL model; however, small N results in large standard errors for the maximum-likelihood estimates of p and c (Table 1). Seven foreshocks were identified within a 0.015-day period prior to the mainshock; land-based networks recorded two of these.

3.3. Endeavour segment of the Juan de Fuca Ridge—08 June 1999

The sequence began with a magnitude $3.9m_b$ (REB) ($3.4m_b$ PDE) earthquake at 20:14Z on 08 June 1999 near $47^\circ 50'$ N. Johnson et al. (2000) report a normal-faulting mechanism for the initial shock and a larger moment magnitude ($4.5M_w$). The event was located ~ 7.5 km west of the present spreading axis, with the majority of the events detected by SOSUS also located to the west of the axis (Fig. 3c). The sequence produced changes in vent temperature at several hydrothermal sites within the axial valley, as discussed by Johnson et al. (2000). It also may have disrupted the hydrothermal system as far away as Axial Volcano, some 220 km to the south (Johnson et al., 2001).

SLC analysis selected 474 aftershocks within ~ 14 days of the mainshock using the $D=4.8$ ST-km criterion (Fig. 6). At least four of these events are listed in the PDE catalog. They occur at 0.19, 0.95, 1.80 and 1.84 days following the initial shock, with magnitudes of 3.9, 4.2, 3.4 and $4.0m_b$, respectively. M_c is 204 db and $b_t=0.069$. SLC analysis with the $D_c=7.5$ ST-km criterion selected 506 aftershocks within 16.5 days, including an additional teleseismi-

cally recorded event 12.47 days after the mainshock. Only the June 9th events ($t=0.19$ and 0.95 days) are reported by the PIDC. They also assign the largest relative magnitude ($4.5m_b$) to the $t=0.95$ day event.

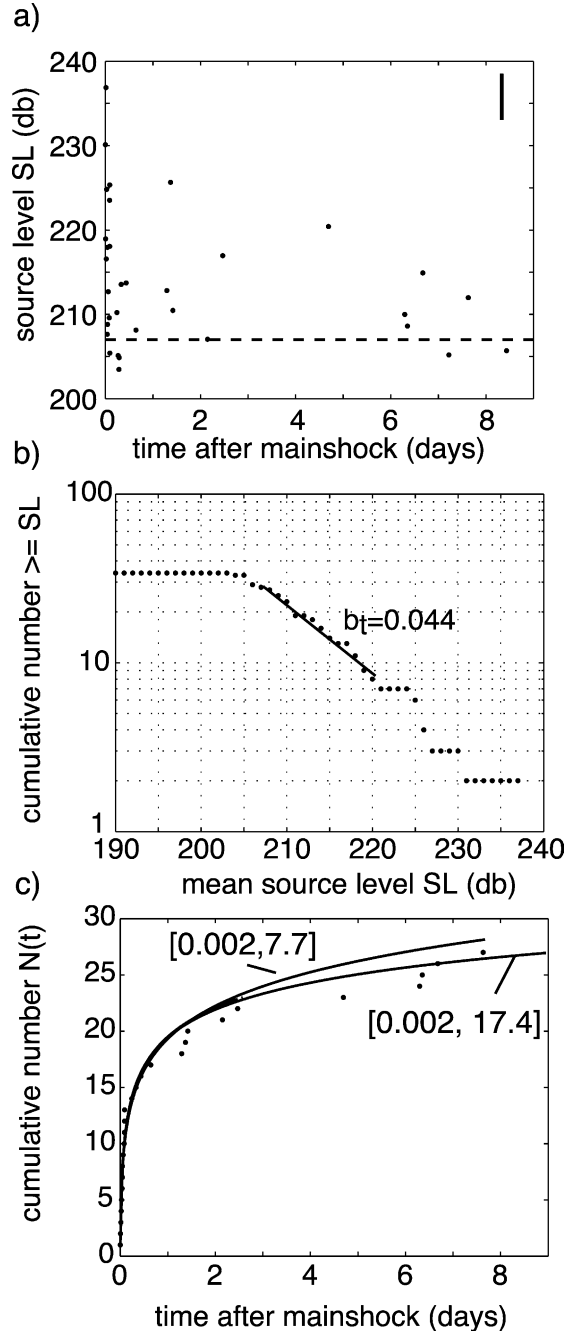


Fig. 7. Aftershock sequence initiated on 23 August 1996, near 4° S on the Discovery Transform of the EPR. The events selected using the $D_c=7.5$ ST-km criterion are shown. (a) Source level vs. time relative to the mainshock. Vertical bar is the median source level error. Events with source levels ≥ 207 db (horizontal line) are used in determining the parameters of the MOL. (b) Cumulative-source level plot of aftershocks. $M_c=207$ db. $b_t=0.044$. (c) Cumulative number of events vs. time after the mainshock. Solid line is the predicted cumulative distribution for the maximum-likelihood estimates of the MOL parameters, as given in Table 2 (Dashed where extrapolated). The data are fit well by a MOL model.

A maximum-likelihood estimate cannot be obtained for either D_c criterion (4.8 or 7.5 ST-km) with $S < 0.7$, due to anomalous behavior during first day (see inset Fig. 6c). For $S > 0.7$, the best-fitting values of p , c and K are all unusually large, with $p > 3$, $c > 2$ and $K > 10^3 - 10^4$ (Table 1). Anderson–Darling statistics indicate the sequence is poorly described by a MOL model, with A^2 values suggesting the proposed distribution can be rejected with $\gg 95\%$ confidence (Table 1). For the period 0.1–2.25 days, the data are better fit by a constant event rate, which might be applicable for some types of submarine volcano-tectonic sequences (e.g., Tolstoy et al., 2001) ($A^2 = 2.55$). Choosing a longer duration series by selecting all events within 40 km for the mainshock during a period of 80 days (Fig. 6c) yields a lower p -value estimate, but provides a worse fit to the data (Table 1).

4. Transform sequences

4.1. Discovery Transform (4°S EPR)—23 August 1996

The 75-km-long Discovery Transform near 4°S on the EPR consists of two closely spaced left-stepping segments separated by a ~ 8 km long intra-transform spreading center (Searle, 1983). The mainshock, a $5.9M_w$ left-lateral strike-slip event, occurred on 23 August 1996 near $104^\circ 25' \text{W}$. The sequence is confined to the western portion of the transform—between the EPR axis and the intra-transform spreading center (Fig. 3d). In addition to

the mainshock, a $5.8M_w$ teleseismically recorded event occurred at 0.016 days after the mainshock (Fig. 7).

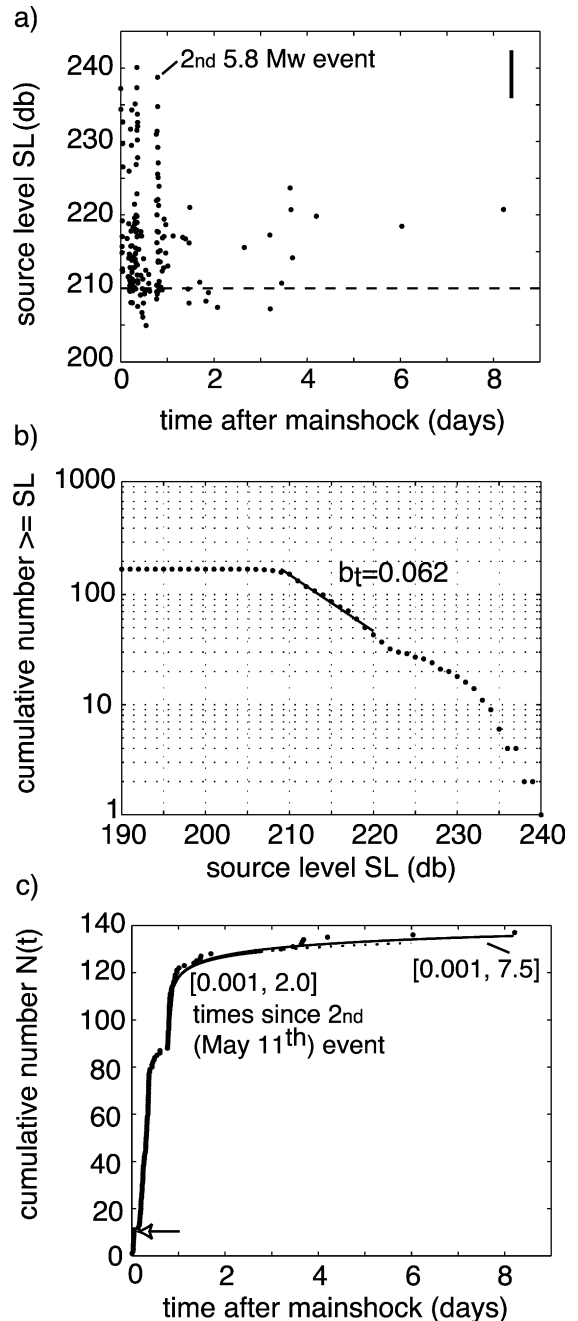


Fig. 8. Aftershock sequence initiated on 10 May 1998, near $8^\circ 20' \text{N}$ on the Siqueiros Transform of the EPR. The events selected using the $D_c = 7.5$ ST-km criterion are shown. Sequence contains two $5.8M_w$ events. (a) Median source level vs. time relative to the mainshock. Vertical bar is the median source level error. Events with source levels ≥ 209 db (horizontal line) are used in determining the parameters of the MOL. (b) Cumulative-source level plot of aftershocks. $M_c = 209$ db. $b_t = 0.062$. (c) Cumulative number of events vs. time after the mainshock. Solid line is the predicted cumulative distribution for the maximum-likelihood estimates of the MOL parameters (Dashed where extrapolated). The horizontal arrow marks a small data gap. Only the data following the second $5.8M_w$ event are modeled. Time intervals are listed relative to this event, as in Table 2. The data are fit well by a MOL model.

SLC analysis selected 34 events during a period of ~ 8 days using the $D_c=7.5$ ST-km criterion and 37 events during a ~ 17 -day period using the $D_c=12.0$ ST-km criterion. The data are complete for $SL>207$ db, with $b_t=0.044$. The p -value is estimated to be 0.96–1.05, with the event distribution described well by the MOL. SLC analysis identified three foreshocks within 0.009 days of the mainshock.

4.2. Siqueiros Transform ($8^\circ 20' N$ EPR)—10 May 1998

The Siqueiros Transform consists of four right-stepping transform segments separated by three intra-transform spreading centers (Pockalny et al., 1997). During May 1998, a cluster of earthquakes that contained two right-lateral $5.8M_w$ events—separated by 0.79 days—occurred along the eastern-most segment of the transform. The first of these two largest events occurred on May 10th and was located near the ridge-transform intersection. The second occurred on May 11th and was located further west, mid-way between the EPR axis and eastern most intra-transform spreading center (Fig.

3e). Five additional teleseismic events with magnitudes 4.0–4.7 m_b were reported by both the NEIC and PIDC, with three additional small ($<4.0m_b$) events reported by the PIDC. All of these teleseismically reported events occur temporally between the two $5.8M_w$ events.

SLC analysis identified 169 aftershocks within the sequence during a period of ~ 8 days using the 7.5 ST-km criterion and 176 aftershocks during a period of ~ 17 days using the $D=12$ ST-km criterion. The sequence has $M_c=210$ db, with $b_t=0.062$ (Fig. 8b). Due to a small data gap near the beginning of the sequence and the small timing difference between the two large events (Fig. 8c), only the data following the second $5.8M_w$ event was fit by the MOL. The estimated decay parameters for these data are listed in Table 2. The p -values are estimated to be near 1.0, with the data fit well by the MOL model.

4.3. Western Blanco Transform ($44^\circ N$ JdFR)—02 June 2000

The ~ 350 km long right-lateral Blanco Transform in the northeast Pacific Ocean connects the JdF

Table 2
Properties of aftershock sequences associated with oceanic-transforms

Sequence	D_c^a	$[S, T]^b$ (days)	N_u^c	p	c (days)	K	A^2^d	
Discovery $4^\circ S$ EPR 23 Aug 96 $5.9M_w^e$	7.5	[0.002, 7.7]	27	0.96 (0.16) ^f	0.006 (0.013)	4.2	0.67	
		[0.002, 2.5]	22	1.05 (0.28)	0.01 (0.02)	3.8	0.47	
Siqueiros $8^\circ 20' N$ EPR 11 May 98 $5.8M_w^e$	12.0	[0.002, 17.4]	28	1.06 (0.15)	0.01 (0.02)	3.7	0.37	
		7.5	[0.001, 7.5]	41	1.09 (0.12)	0.005 (0.006)	5.0	0.26
			[0.001, 2.0]	33	1.29 (0.25)	0.01 (0.01)	3.4	0.21
W. Blanco $44^\circ 20' N$ 02 Jun 00 JdFR $6.2M_w^e$	12.0	[0.001, 16.2]	43	1.12 (0.11)	0.006 (0.006)	4.7	0.30	
		7.5	[0.001, 8.6]	43	1.15 (0.12)	0.005 (0.005)	4.4	0.85
			[0.001, 2.4]	40	1.07 (0.15)	0.003 (0.004)	5.3	0.49
		12.0	[0.001, 42.8]	51	1.11 (0.08)	0.004 (0.004)	5.0	0.48
			[0.001, 8.6]	45	1.15 (0.12)	0.005 (0.005)	4.8	0.27
		[0.001, 2.4]	42	1.04 (0.14)	0.003 (0.004)	5.9	0.70	

^a Space–time metric used to select aftershocks using SLC analysis.

^b Time interval during which the data are modeled. Times are relative to mainshock time. The full duration data, as determined from SLC analysis, were modeled for all sequences. Numerous other time intervals, chosen by inspection of the aftershock data, were also modeled; only values relevant to the discussion are reported.

^c Number of aftershocks within the interval $[S, T]$ used in determining p , c and K .

^d Anderson–Darling statistic. Smaller values of A^2 indicate better fits to the MOL. Sequences with $A^2 < \sim 1.0$ are fit well by the MOL model.

^e Mainshock magnitude.

^f Standard error of the maximum likelihood estimation.

and Gorda Ridges. The fault consists of five major right-stepping transform segments. These segments are bounded by a series of extensional basins or depressions, which resemble pull-apart basins described in numerous continental settings (Embley and Wilson, 1992). In June 2000, a series of earthquakes occurred along the western-most Blanco Transform segment between the JdFR and the East Blanco Depression (Dziak et al., 2001).

The mainshock occurred at 11:13Z on June 2 and had a magnitude of $6.2M_w$. SLC analysis identified 68 aftershocks during ~ 8.5 days using the 7.5 ST-km criterion and 83 events during ~ 43 days using the 12.0 ST-km criterion. M_c is estimated to be 212 db, with $b_t = 0.061$. Events selected using the latter criterion are shown in Fig. 3f. The data are well fit

($A^2 < 1.0$) with p -values in the range of 1.04–1.15 for durations of 2.4–42.8 days. Several foreshocks were identified as well, with foreshock activity concentrated near 0.3 days prior to the mainshock (Fig. 9d).

5. An oceanic thrust sequence

5.1. Northern edge of the Easter Microplate—5 September 1996

The Easter Microplate is centered near 25°S on the EPR and bounded by the Pacific Plate to the west and the Nazca Plate to the east. It is subject to a clockwise rotation, which gives rise to a zone of compression

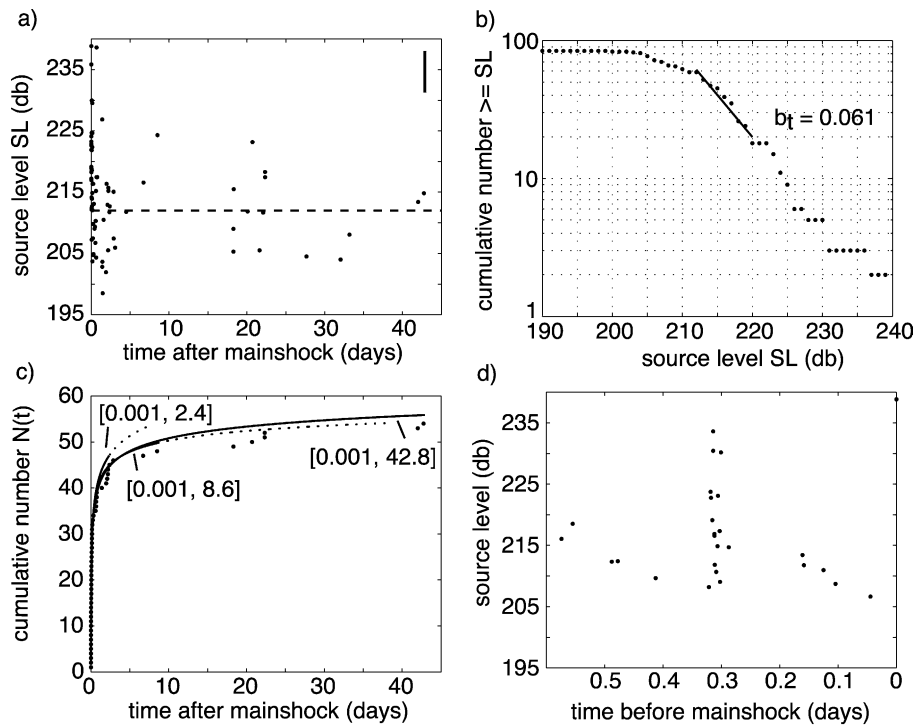


Fig. 9. Aftershock sequence initiated on 2 June 2000, on the western Blanco Transform on the JdFR. The events selected using the $D_c = 12.0$ ST-km criterion are shown. (a) Source level vs. time relative to the mainshock. Vertical bar is the median source level error. Events with source levels ≥ 212 db (horizontal line) are used in determining the parameters of the MOL. (b) Cumulative-source level plot of aftershocks. $M_c = 212$ db. $b_t = 0.061$. (c) Cumulative number of events vs. time after the mainshock. Solid line is the predicted cumulative distribution for the maximum-likelihood estimates of the MOL parameters, as given in Table 2 (Dashed where extrapolated). Data are fit well by the MOL model. (d) Foreshock source level vs. time before the mainshock.

along its northwestern boundary. Compressional deformation is manifested as a series of elongate ridges, which are thought to represent fault propaga-

tion folds associated with north-dipping thrust faults (Rusby and Searle, 1993) (Fig. 10).

On 05 September 1996, a $7.1M_s$ thrust occurred in this region of compressional deformation—near $21^\circ 30' S$, $112^\circ 45' W$ (Fig. 3g). The focal mechanism of Delouis et al. (1998) is consistent with slip along a plane dipping at 15° to the N–NE. SLC cluster analysis selected 192 aftershocks with a duration of ~ 26 days using the $D_c = 20$ ST-km criterion and 195 aftershocks with a duration of ~ 40 days using the $D_c = 31$ ST-km criterion. (Note that the large D_c values used for this region reflect its position relative to the array and our reduced capability to detect and accurately locate events in the region.) No foreshocks were identified. M_c is 210 db and b_t is 0.079. In addition to the mainshock, four aftershocks were detected teleseismically at 0.03, 0.04, 0.06 and 7.19 days following the mainshocks. The 0.06-day event was the largest, having a magnitude of $6.2M_w$. The p -value is estimated to be 1.02–1.23, with the data well described by the MOL (Table 3).

This region lies well to the south of the Pacific AUH array; therefore, location errors are several times greater than within the array and the actual error field is expected to be elliptical with the long axis oriented toward the array (N–NE in this case) (Fox et al., 2001). Nonetheless, aftershocks are distributed largely to the immediate north of a large compression ridge, which may represent the surface expression of a shallow north-dipping thrust fault (Fig. 3g) (Rusby and Searle, 1993). The location and spatial distribution of the aftershocks are roughly consistent with the likely dimensions of the rupture. Moreover, the mainshock epicenter is located toward the northern limit of the aftershock distribution, ~ 90 km from the com-

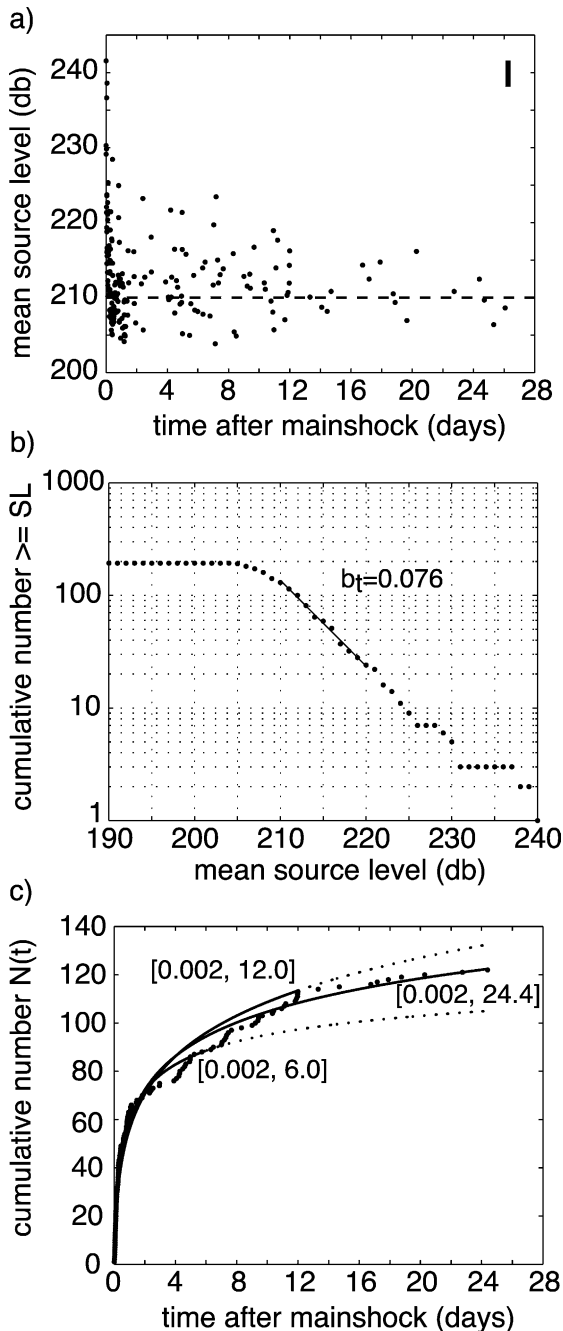


Fig. 10. Aftershock sequence initiated on 5 September 1996, near $23^\circ S$ on the northern edge of the Easter Microplate. The events selected using the $D_c = 20$ ST-km criterion are shown. (a) Mean source level vs. time relative to the mainshock. Vertical bar is the median source level error. Events with source levels ≥ 210 db (horizontal line) are used in determining the parameters of the MOL. (b) Cumulative-source level plot of aftershocks. $M_c = 210$ db. $b_t = 0.076$. (c) Cumulative number of events vs. time after the mainshock. Solid line is the predicted cumulative distribution for the maximum-likelihood estimates of the MOL parameters, as given in Table 3 (Dashed where extrapolated). The data are fit well by the MOL model.

Table 3
Properties of the 1996 Easter Microplate aftershock sequence

Sequence	D_c^a	$[S, T]^b$ (days)	N_u^c	p	c (days)	K	A^2 ^d
Easter Microplate 21°30' S EPR 7.1 M_s^c	20.0	[0.002, 24.4]	122	1.02 (0.11) ^f	0.07 (0.05)	21.1	0.84
		[0.002, 6.0]	88	1.23 (0.23)	0.12 (0.09)	21.0	0.82
	31.0	[0.002, 40.4]	125	1.10 (0.09)	0.10 (0.05)	22.0	0.94

^a Space–time metric used to select aftershocks using SLC analysis.

^b Time interval during which the data are modeled. Times are relative to mainshock time. The full duration data, as determined from SLC analysis, were modeled for all sequences. Numerous other time intervals, chosen by inspection of the aftershock data, were also modeled; only values relevant to the discussion are reported.

^c Number of aftershocks within the interval $[S, T]$ used in determining p , c and K .

^d Anderson–Darling statistic. Smaller values of A^2 indicate better fits to the MOL. Sequences with $A^2 < \sim 1.0$ are fit well by the MOL model.

^e Mainshock magnitude.

^f Standard error of the maximum likelihood estimation.

pressional ridge. This is consistent with the initiation of the rupture at depth.

6. Discussion and summary

For remote portions of the mid-ocean ridge system, hydroacoustic monitoring greatly improves our ability to detect and locate earthquakes, relative to global seismic networks, with an increase of ~ 1.5 – 2.0 orders of magnitude in the completeness level of the earthquake catalog. In recent years, several large earthquake sequences have been recorded by AUH and SOSUS arrays along portions of the slow-spreading MAR, intermediate-spreading JdFR and fast-spreading EPR. We have examined the characteristics of seven well-recorded sequences, which qualitatively appear to be tectonic in origin—those containing a large magnitude earthquake that is followed by a series of events with rapidly decaying event rate.

6.1. Decay constant of a modified Omori law

Six of the seven sequences examined are well described by the MOL model. Three well-described sequences occurring along the Siqueiros, Discovery and Blanco Transforms exhibit $p = 0.94$ – 1.29 . Similarly, a well-described sequence associated with a low-angle thrust event near the northern edge of the Easter Microplate exhibits $p = 1.02$ – 1.12 . All of these values are consistent with those typically observed in continental lithosphere exhibiting average heat flow (e.g., Kisslinger and Jones, 1991; Utsu et al., 1995).

Although the number of ridge crest sequences is limited, due to the low abundance of large magnitude normal-faulting events in the fast- and intermediate-spreading environments and the infancy of monitoring along the slow-spreading MAR, there is some indication of higher p -values in this setting. Maximum-likelihood estimates of p for an April 1999 MAR sequence within the lower rift mountains are 1.57 ± 0.25 and 1.74 ± 0.23 for the two event selection criteria used. A high p -value (2.37 ± 1.65) also is suggested for a February 2000 sequence, which occurs primarily on the median valley floor of the MAR. Both sequences are fit well by a MOL model; however, a large standard error is associated with the latter estimate because the number of aftershocks is small. A third normal-faulting sequence on the Endeavour segment of the JdFR is fit poorly by the MOL; therefore, its large estimated p -value (>3.0) may have little significance.

The different p -values observed for ridge and transform sequences may reflect lower hypocentral temperatures within the transform setting—a potential consequence of reduced asthenospheric upwelling, which lowers the advection of heat and suppresses the production of melt, and enhanced hydrothermal cooling associated with pervasive fracturing along the transforms (e.g., Phipps Morgan and Forsyth, 1988; Blackman and Forsyth, 1992). As monitoring on the slow-spreading MAR continues and expands, hydroacoustic data may allow us to confirm or refute the proposed correlation between heat flow and p -value (e.g., Mogi, 1967; Kisslinger and Jones, 1991). In addition, further 3-D modeling of ridge-transform

thermal structure is needed to better predict the expected differences in temperatures between transform and near-axis environments.

6.2. Spatial distribution of events within the sequences

Although hydroacoustic locations may not correspond precisely to seismically determined epicenters, event locations do not appear to be broadly biased with regard to large-scale topographic features. All three transform sequences appear to be restricted to individual segments of the fault, bounded by the ridge axis and intra-transform spreading centers. Intra-transform spreading segments, therefore, may act as barriers to rupture and consequently serve to limit the maximum size of an earthquake along the transform (Dziak et al., 1991).

Aftershocks following a 7.1 M_s thrust event on the northern edge of the Easter Microplate are distributed to the immediate north of a large compression ridge. This ridge may represent the surface expression of the north-dipping thrust along which the rupture occurred. The distribution of aftershocks and the location of the mainshock are consistent with the likely dimensions of the rupture and the shallow thrust mechanism of Delouis et al. (1998).

Aftershocks associated with normal-faulting events on the MAR are confined to within ~ 20 km of the mainshock. The trend of their spatial distribution parallels that of the ridge axis and the structural fabric of the seafloor. They occur on the lower bounding walls and valley floor, within the region where most seismic activity is confined (Smith et al., in press).

6.3. Size–frequency distributions

The size–frequency distribution of earthquakes can be expressed in terms of acoustic source level, where $\log N(\text{SL})$ is proportional to $-b_t \text{SL}$. For the AUH datasets from the equatorial Pacific and Atlantic Oceans, the three dip–slip sequences have larger b_t values than do the two strike–slip sequences, 0.083 ± 0.016 vs. 0.053 ± 0.023 . Similar differences in b_t are observed within the normal-faulting dominated MAR and strike–slip dominated EPR AUH catalogs as a whole (i.e., excluding the sequences). These differences are consistent with the variation in seismic b -value reported in the mid-ocean ridge set-

ting, with higher b -values along spreading-centers relative to transforms (Francis, 1968; Molchan et al., 1997). The Endeavour (normal-faulting) and western Blanco (strike–slip) sequences, however, do not have significantly different b_t values—as estimated using SOSUS data. Although b_t may reflect the local or regional tectonic setting, we cannot rule out some variability in the T-wave generation process, which would not reflect the earthquake process itself. For example, Dziak (2001) has shown empirically that for a given magnitude earthquake, T-wave energy is lower for dip–slip than for strike–slip events. Conceivably, the relative efficiency of dip–slip and strike–slip T-wave generation could vary with event size, resulting in different b_t slopes.

6.4. The 08 June 1999 Endeavour sequence

The 08 June 1999 Endeavour Segment sequence has attracted much attention due to its correlation with changes in vent temperature and chemistry 4–11 days after initiation of the sequence at distances of 7–10 km within the axial valley of the Endeavour Segment (Johnson et al., 2000) and possibly more than 200 km away at Axial Volcano (Johnson et al., 2001). The Endeavour sequence was initiated by a moderate-size earthquake (magnitude 3.4–4.5 as reported by various agencies)—contributing to the suggestion that it may be of tectonic origin (Johnson et al., 2000). However, the event distribution is not described satisfactorily by the MOL, as might be expected if the activity simply represented the relaxation of stresses associated with the mainshock. Instead, we find the first ~ 2.25 days of the sequence are fit substantially better by a constant event rate, as might be applicable for seismic sequences associated with some volcanic spreading events (Tolstoy et al., 2001). Based on the magnitudes assigned within the REB and PDE catalogs, at least four earthquakes having a size approximately equal to, or slightly greater than, the initial shock occurred during the first 2 days. Inspection of the source level vs. time data (Fig. 6a) indicates that no single event dominates the sequence and that none of the largest aftershock events are associated with pronounced changes in event rate—as observed, for example, in the 16°35' N sequence on the MAR and the Siqueiros sequence on the EPR. The absence of a dominant event and the succession of similar-size events are

consistent with volcanic seismicity reported in a number of environments (e.g., Mogi, 1963; Sykes, 1970; Benoit and McNutt, 1996; Tolstoy et al., 2001). Moreover, the sequence contains an anomalous number of events given the size of its proposed mainshock, with ~ 500 events selected from SLC analysis of the raw SOSUS data. Similar-sized mainshocks (i.e., events initiating MOL-sequences) on the JdFR and MAR, for example, typically produce over an order of magnitude fewer aftershocks of sufficient size to be detected by hydroacoustic networks. The along-axis extent of activity, which is well constrained, also appears to be significantly (>2 times) larger than that observed for normal-faulting sequences on the MAR (compare Fig. 3a and b with c).

The distribution, timing and abundance of events argue that the June 8th sequence is not a simple tectonic aftershock sequence. Rather, the observed seismicity and hydrothermal vent anomalies (Johnson et al., 2001) may reflect the response of the lithosphere to the emplacement or movement of magma at depth. It is noteworthy that the June 1999 sequence overlaps spatially with a January 2000 swarm (lacking a dominant mainshock event) that contains >200 SOSUS-detected earthquakes. Repeated swarm activity is a phenomenon commonly associated with a volcanic/magmatic activity.

7. Conclusions

Hydroacoustic data constrain the origin time and T-wave epicenter locations of earthquakes occurring along the mid-ocean ridge system. Such information can be used to study the clustering properties of seismicity and estimate the temporal properties of aftershock sequences. Six of the seven earthquake sequences examined in this study are described well by the MOL, with an event rate decaying as $\sim 1/t^p$ for times following the mainshock. The nature of these sequences could not be discerned from the teleseismic record alone, due to the limited number of events detected by land-based stations.

Four aftershock sequences along oceanic-transform faults, and one sequence associated with the compressional edge of an oceanic microplate, exhibit p -values consistent with the global average (Utsu et al., 1995), ~ 1.0 – 1.2 . These p -values are slightly larger than the

0.928 ± 0.024 obtained for a stacked sequence (Davis and Frohlich, 1991), which contained events detected teleseismically from multiple ridge and transform sequences. A normal-faulting sequence along western median valley wall near 24°N on the MAR, which is well described by the MOL, exhibits a higher p -value of ~ 1.57 – 1.74 . A higher p -value, 2.37 ± 1.65 , also is suggested for a sequence near 16°N occurring on the median valley floor of the MAR, but this maximum-likelihood estimate is constrained less tightly because of the small number of aftershocks. Continued observation will be needed to determine if higher p -values are characteristic of all median valley sequences. Higher p -values along the ridge crest, relative to the transforms and many other settings, might be consistent with the proposed correlation between hypocentral temperature and p -value, with higher temperatures associated with the spreading centers.

The MOL cannot describe adequately a large sequence of events that was initiated on 8 June 1999 along the Endeavour Segment of the JdFR. Given the moderate magnitude of the largest events, the sequence contains a clearly anomalous number of events—more than 1 order of magnitude more than expected. Neither the initial earthquake, nor subsequent events of similar size, can be shown to dominate the sequence. These observations are inconsistent with an aftershock sequence and suggest that the observed seismic activity and hydrothermal vent anomalies may reflect the response of the lithosphere to magmatic activity, rather than solely its response to changes in stress associated with a tectonic earthquake.

Acknowledgements

This work would not have been possible without the skillful efforts of H. Matsumoto, who designed the AUHs, and T-K Lau who developed the location and analysis software used at the NOAA/OSU acoustics laboratory in Newport. M. Fowler and P. Will did an outstanding job deploying and recovering the AUHs in the Atlantic and Pacific. We also greatly appreciate the efforts of S. Follet, M. Fowler, J. Getsiv, and P. Will for processing most of the AUH hydrophone data utilized in this study. We thank Y. Ogata and T. Utsu for making their maximum-likelihood routines available. D.R.B. was supported partially by the DEES at

Columbia University. Discussions with D. Blackman, S. Carbotte, M. Kleinrock, W. Menke, J. Nagel and C. Scholz are gratefully acknowledged. Reviews by F. Duennebieer and L. Dorman were helpful in improving this manuscript. Data collection and analysis in the Atlantic was supported by NSF grant OCE9812237. North Pacific (SOSUS) and equatorial Pacific (AUH) data collection and analysis were supported by the National Ocean Partnership Program and the NOAA Vents Program, PMEL contribution number 2422. LDEO contribution number 6341.

References

- Akaike, H., 1973. A new look at statistical model identification. *IEEE Trans. Autom. Control* 19, 716–723.
- Anderson, D.A., Darling, D.A., 1954. A test of goodness of fit. *J. Am. Stat. Soc.* 49, 765–769.
- Benoit, J.P., McNutt, S.R., 1996. Global volcanic earthquake swarm database and preliminary analysis of volcanic earthquake swarm duration. *Ann. Geofis.* 39, 221–229.
- Bergman, E.A., Solomon, S.C., 1984. Source mechanisms of earthquakes near mid-ocean ridges from body waveform inversion: implications for the early evolution of oceanic lithosphere. *J. Geophys. Res.* 89, 11415–11441.
- Blackman, D.K., Forsyth, D.W., 1992. The effect of plate thickening on three-dimensional, passive flow of the mantle beneath mid-ocean ridges. In: Phipps Morgan, J., Blackman, D.K., Sinton, J.M. (Eds.), *Mantle Flow and Melt migration at Mid-Ocean Ridges*. *Geophys. Monograph*, vol. 71. Am. Geophys. Union, Washington, DC, pp. 311–326.
- Creamer, F.H., 1994. The relationship between temperature and the decay parameter for aftershock sequences near Japan. PhD Thesis, University of Colorado, Boulder.
- Creamer, F.H., Kisslinger, C., 1993. The relationship between temperature and the decay parameter for aftershock sequences near Japan. *EOS, Trans. Am. Geophys. Union* 74, F417.
- Davis, S.D., Frohlich, C., 1991. Single-link cluster analysis, synthetic earthquake catalogues, and aftershock identification. *Geophys. J. Intern.* 104, 289–306.
- Delouis, B., Nicolas, A., Ildefonse, B., Philip, H., 1998. Earthquake focal mechanism and ocean thrust near Easter Microplate: analogy with Oman ophiolite. *Geophys. Res. Lett.* 25, 1443–1446.
- Dieterich, J., 1994. A constitutive law for rate of earthquake production and its application to earthquake clustering. *J. Geophys. Res.* 99, 2601–2618.
- Dziak, R.P., 2001. Empirical relationship of T-wave energy and fault parameters of northeast Pacific Ocean earthquakes. *Geophys. Res. Lett.* 28, 2537–2540.
- Dziak, R.P., Fox, C.G., 1999. The January 1998 earthquake swarm at Axial Volcano, Juan de Fuca Ridge: hydroacoustic evidence of seafloor volcanic activity. *Geophys. Res. Lett.* 26, 3429–3432.
- Dziak, R.P., Fox, C.G., Embley, R.W., 1991. Relationship between the seismicity and geologic structure of the Blanco transform fault zone. *Mar. Geophys. Res.* 13, 203–208.
- Dziak, R.P., Fox, C.G., Embley, R.W., Lupton, J.E., Johnson, G.C., Chadwick, W.W., Koski, R.A., 1996. Detection of and response to a probable volcanogenic T-wave event swarm on the western Blanco Transform. *Geophys. Res. Lett.* 23, 873–876.
- Dziak, R.P., Fox, C.G., Matsumoto, H., Schreiner, A.E., 1997. The April 1992 Cape Mendocino earthquake sequence: seismo-acoustic analysis utilizing fixed hydrophone arrays. *Mar. Geophys. Res.* 19, 137–162.
- Dziak, R.P., Chadwick, W.W., Embley, R.W., Fox, C.G., Hammond, S.R., 2001. Temperature changes at south Cleft, Juan de Fuca Ridge, associated with Blanco Transform seismicity: more evidence of far-field effects induced by earthquakes. *Eos Trans. AGU* 82 (47) Fall Meet. Suppl., Abstract S21A-06.
- Dziewonski, A.M., Chou, T.-A., Woodhouse, J.H., 1981. Determination of earthquake source parameters from waveform data for studies of global and regional seismicity. *J. Geophys. Res.* 86, 2825–2852.
- Embley, R.W., Wilson, D.S., 1992. Morphology of the Blanco transform fault zone, NE Pacific: implications for its tectonic evolution. *Mar. Geophys. Res.* 14, 25–45.
- Fox, C.G., 1995. Special collection on the June 1993 volcanic eruption on the CoAxial segment, Juan de Fuca Ridge. *Geophys. Res. Lett.* 22, 129–130.
- Fox, C.G., Dziak, R.P., 1998. Hydroacoustic detection of volcanic activity on the Gorda Ridge. *Deep-Sea Res.* 45, 2513–2530.
- Fox, C.G., Dziak, R.P., Matsumoto, H., Schreiner, A.E., 1994. Potential for monitoring low-level seismicity on the Juan de Fuca Ridge using military hydrophone arrays. *Mar. Technol. Soc. J.* 27, 22–30.
- Fox, C.G., Matsumoto, H., Lau, T.-K.A., 2001. Monitoring Pacific Ocean seismicity from an autonomous hydrophone array. *J. Geophys. Res.* 106, 4183–4206.
- Francis, T.J.G., 1968. Seismicity of mid-oceanic ridges and its relation to properties of the upper mantle and crust. *Nature* 220, 899–901.
- Francis, T.J.G., Porter, I.T., 1971. A statistical study of Mid-Atlantic Ridge earthquakes. *Geophys. J. R. Astron. Soc.* 24, 31–50.
- Frohlich, C., 1987. Aftershocks and temporal clustering of deep earthquakes. *J. Geophys. Res.* 92, 13944–13956.
- Frohlich, C., Davis, S.D., 1990. Single-link cluster analysis as a method to evaluate spatial and temporal properties of earthquake catalogues. *Geophys. J. Intern.* 100, 19–32.
- Geller, R.J., 1976. Scaling relations for earthquake source parameters and magnitudes. *Bull. Seismol. Soc. Am.* 66, 1501–1523.
- Johnson, H.P., Hutnak, M., Dziak, R.P., Fox, C.G., Urcuyo, I., Cowen, J.P., Nabelek, J., Fisher, C.R., 2000. Earthquake-induced changes in a hydrothermal system on the Juan de Fuca mid-ocean ridge. *Nature* 407, 174–177.
- Johnson, H.P., Dziak, R.P., Fisher, C.R., Fox, C.G., Pruis, M.J., 2001. Earthquakes' impact on hydrothermal systems may be far-reaching. *EOS, Trans. Am. Geophys. Union* 82, 233–236.
- Kisslinger, C., 1996. Aftershocks and fault zone properties. *Adv. Geophys.* 38, 1–36.
- Kisslinger, C., Jones, L.M., 1991. Properties of aftershock sequences in Southern California. *J. Geophys. Res.* 96, 11947–11958.

- Lewis, P.A.W., 1961. The distribution of the Anderson–Darling statistic. *Ann. Math. Stat.* 32, 1118–1123.
- Mogi, K., 1963. Some discussions on aftershock, foreshock and earthquake swarms—the fracture of a semi-infinite body caused by inner stress origin and its relation to the earthquake phenomena. *Bull. Earthquake Res. Inst., Univ. Tokyo* 41, 615–658.
- Mogi, K., 1967. Earthquakes and fractures. *Tectonophysics* 5, 35–55.
- Molchan, G., Kronrad, T., Panza, G.F., 1997. Multi-scale seismicity model of seismic risk. *Bull. Seismol. Soc. Am.* 87, 1220–1229.
- Nanjo, K., Nagahama, H., Satomura, M., 1998. Rates of aftershock decay and the fractal structure of active fault systems. *Tectonophysics* 287, 173–186.
- Nyffenegger, P., 1998. Aftershock occurrence rate decay for individual sequences and catalogs. PhD Thesis, University of Texas.
- Nyffenegger, P., Frohlich, C., 1998. Recommendations for determining p values for aftershock sequences and catalogs. *Bull. Seismol. Soc. Am.* 88, 1144–1154.
- Nyffenegger, P., Frohlich, C., 2000. Aftershock occurrence rate decay properties for intermediate and deep earthquake sequences. *Geophys. Res. Lett.* 27, 1215–1218.
- Ogata, Y., 1983. Estimation of the parameters in the modified Omori formula for aftershock frequencies by the maximum likelihood procedure. *J. Phys. Earth* 31, 115–124.
- Ogata, Y., 1999. Seismicity analysis through point-process modeling: a review. *PAGEOPH* 155, 471–508.
- Park, M., Odom, R.I., Soukup, D.J., 2001. Model scattering: a key to understanding oceanic T-waves. *Geophys. Res. Lett.* 28, 3401–3404.
- Phipps Morgan, J., Forsyth, D.W., 1988. Three-dimensional flow and temperature perturbations due to a transform offset: effects on oceanic crustal and mantle structure. *J. Geophys. Res.* 93, 2955–2966.
- Pockalny, R.A., Fox, P.J., Fornari, D.J., Macdonald, K.C., Perfit, M.R., 1997. Tectonic reconstruction of the Clipperton and Siqueiros Fracture Zones: evidence and consequences of plate motion change for the last 3 Myr. *J. Geophys. Res.* 102, 3167–3181.
- Rabinowitz, N., Steinberg, D.M., 1998. Aftershock decay of three recent strong earthquakes in the Levant. *Bull. Seismol. Soc. Am.* 88, 1580–1587.
- Reasenber, P.A., 1985. Second-order moment of Central California seismicity, 1969–1982. *J. Geophys. Res.* 90, 5479–5495.
- Rusby, R.I., Searle, R.C., 1993. Intraplate thrusting near the Easter Microplate. *Geology* 21, 311–314.
- Scholz, C.H., 1990. *The Mechanics of Earthquakes and Faulting*. Cambridge Univ. Press, Cambridge, UK, p. 439.
- Schreiner, A.E., Fox, C.G., Dziak, R.P., 1995. Spectra and magnitude of T-waves from the 1993 earthquake swarm on the Juan de Fuca Ridge. *Geophys. Res. Lett.* 22, 139–142.
- Searle, R.C., 1983. Multiple, closely spaced transform faults in fast-slipping fracture zones. *Geology* 11, 607–610.
- Slack, P.D., Fox, C.G., Dziak, R.P., 1999. P wave detection thresholds, Pn velocity estimates and T wave location uncertainty from oceanic hydrophones. *J. Geophys. Res.* 104, 13061–13073.
- Smith, D.K., Tolstoy, M., Fox, C.G., Bohnenstiehl, D.R., Matsumoto, H., Fowler, M.J., 2002. Hydroacoustic monitoring of seismicity at the slow-spreading Mid-Atlantic Ridge. *Geophys. Res. Lett.* 2001GL013912.
- Sohn, R.A., Hildebrand, J.A., Webb, S.C., 1999. A microearthquake survey of the high-temperature vent fields on the volcanically active East Pacific Rise. *J. Geophys. Res.* 104, 25367–25377.
- Sykes, L.R., 1970. Earthquake swarms and sea-floor spreading. *J. Geophys. Res.* 75, 6598–6611.
- Tolstoy, I., Ewing, W.M., 1950. The T-phase of shallow-focus earthquakes. *Bull. Seismol. Soc. Am.* 40, 25–51.
- Tolstoy, M., Bohnenstiehl, D.R., Edwards, M.H., Kurras, G.J., 2001. Seismic character of an eruption at the ultra-slow spreading Gakkel Ridge. *Geology* 29, 1139–1142.
- Utsu, T., Ogata, Y., 1997. Statistical analysis of seismicity. In: Healy, J.H., Kelis-Borok, V.I., Lee, W.H.K. (Eds.), *IASPEI Software Library*, vol. 6. IASPEI and Seismol. Soc. Am., El Cerrito, CA, pp. 13–94.
- Utsu, T., Ogata, Y., Matsu'ura, R.S., 1995. The centenary of the Omori formula for a decay law of aftershock activity. *J. Phys. Earth* 43, 1–33.
- Willemann, R.J., Frohlich, C., 1987. Spatial patterns of aftershocks of deep focus earthquakes. *J. Geophys. Res.* 92, 13927–13943.